jove

Real-Time Intravital Multiphoton Microscopy to Visualize Focused Ultrasound and Microbubble Treatments to Increase Blood-Brain Barrier Permeability

Charissa Poon[1,2], **Melina Mühlenpfordt**[*,3], **Marieke Olsman**[*,3], **Spiros Kotopoulis**[4,5], **Catharina de Lange Davies**[3], **Kullervo Hynynen**[1,2,6]

[1] Physical Sciences Platform, Sunnybrook Research Institute [2] Institute of Biomedical Engineering, University of Toronto [3] Department of Physics, Norwegian University of Science and Technology [4] Department of Clinical Medicine, University of Bergen [5] Exact Therapeutics AS [6] Department of Medical Biophysics, University of Toronto

[*] These authors contributed equally

Corresponding Author

Charissa Poon

charissa.poon@mail.utoronto.ca

Citation

Poon, C., Mühlenpfordt, M., Olsman, M., Kotopoulis, S., de Lange Davies, C., Hynynen, K. Real-Time Intravital Multiphoton Microscopy to Visualize Focused Ultrasound and Microbubble Treatments to Increase Blood-Brain Barrier Permeability. *J. Vis. Exp.* (180), e62235, doi:10.3791/62235 (2022).

Date Published

February 5, 2022

DOI

10.3791/62235

URL

jove.com/video/62235

Abstract

The blood-brain barrier (BBB) is a key challenge for the successful delivery of drugs to the brain. Ultrasound exposure in the presence of microbubbles has emerged as an effective method to transiently and locally increase the permeability of the BBB, facilitating para- and transcellular transport of drugs across the BBB. Imaging the vasculature during ultrasound-microbubble treatment will provide valuable and novel insights on the mechanisms and dynamics of ultrasound-microbubble treatments in the brain.

Here, we present an experimental procedure for intravital multiphoton microscopy using a cranial window aligned with a ring transducer and a 20x objective lens. This set-up enables high spatial and temporal resolution imaging of the brain during ultrasound-microbubble treatments. Optical access to the brain is obtained via an open-skull cranial window. Briefly, a 3-4 mm diameter piece of the skull is removed, and the exposed area of the brain is sealed with a glass coverslip. A 0.82 MHz ring transducer, which is attached to a second glass coverslip, is mounted on top. Agarose (1% w/v) is used between the coverslip of the transducer and the coverslip covering the cranial window to prevent air bubbles, which impede ultrasound propagation. When sterile surgery procedures and anti-inflammatory measures are taken, ultrasound-microbubble treatments and imaging sessions can be performed repeatedly over several weeks. Fluorescent dextran conjugates are injected intravenously to visualize the vasculature and quantify ultrasound-microbubble induced effects (e.g., leakage kinetics, vascular changes). This paper describes the cranial window placement, ring

transducer placement, imaging procedure, common troubleshooting steps, as well as advantages and limitations of the method.

Introduction

A key challenge to treating neurological disorders is the presence of the blood-brain barrier (BBB). The BBB limits hydrophilic, charged, polar, and large (> 400 Da) molecules from entering the brain parenchyma[1]. One method currently used to deliver therapeutics across the BBB into the brain parenchyma is to use stereotactic intracranial injections[2]. Other less invasive methods under investigation are hindered by the complexity of the techniques used, such as designing drugs for receptor-mediated delivery across the BBB[3], or are limited in the spatial precision of targeted areas, such as intranasal injections[4] or administration of hyperosmotic solutions[5].

The use of ultrasound in conjunction with systemically injected microbubbles, an ultrasound contrast agent, has been developed as a noninvasive means to transiently increase the permeability of the BBB[6]. By using a focused transducer[7] or a steerable phased array of transducers[8,9], ultrasound can be targeted to selected areas in the brain with millimeter level precision, minimizing off-target effects. Ultrasound-microbubble treatments can be customized to each subject's brain anatomy by using magnetic resonance imaging guidance[7,10,11,12,13,14] or stereotactic frames[15]. Furthermore, the extent of increase in BBB permeability can be controlled in real-time by monitoring acoustic emissions from microbubbles[16,17,18]. Clinical trials investigating the safety and feasibility of ultrasound-microbubble treatments are currently in progress worldwide (e.g., ClinicalTrials.gov identifier NCT04118764).

Ultrasound-microbubble BBB treatments are typically evaluated by confirming treatment induced increases in BBB permeability, visualized in contrast-enhanced magnetic resonance imaging, or by dye extravasation in *in vivo* imaging or *ex vivo* histology. However, most microscopic analyses have been performed *ex vivo*, following the completion of ultrasound-microbubble treatments[11,19], thereby missing the dynamic biological responses during, and immediately following, ultrasound exposure. Real-time imaging conducted during ultrasound exposure may aid in understanding the mechanisms driving ultrasound-microbubble BBB treatments as well as downstream responses, which may increase our understanding of its therapeutic applications. Furthermore, the use of chronic cranial windows with *in vivo* imaging techniques would enable longitudinal studies to evaluate temporal aspects of ultrasound-microbubble treatments.

The goal of this protocol is to describe the surgical and technical procedures required to conduct real-time multiphoton imaging of ultrasound-microbubble treatments for acute and chronic studies in rodents (**Figure 1**). This is achieved in two parts: first, to create a cranial window to enable *in vivo* imaging, and second, to mount a ring transducer on the top to enable concurrent sonication and imaging. Cranial windows have been extensively used by neuroscientists for *in vivo* imaging of neurovascular coupling[20], β-amyloid pathogenesis[21], and neuroimmunology[22], among others. In this protocol, surgical procedures for creating acute (non-recovery) and chronic (recovery) cranial windows in the mouse and rat skull are

described. Cranial window methodologies, particularly for chronic experiments, have been well-documented[23,24,25]. To be consistent with existing literature, the terms 'acute' and 'chronic' will be used throughout this protocol. The design of ring transducers for *in vivo* imaging has also been previously described[26]. Despite the availability of these techniques and the insights that can be gained from real-time imaging of ultrasound-microbubble treatments, there are very few research laboratories that have successfully published literature using this technique[26,27,28,29,30,31,32]. As such, in this protocol, the surgical and technical details of conducting these real-time ultrasound-microbubble experiments are described. While the specified sonication and imaging parameters have been optimized for BBB experiments, other effects of ultrasound exposure to the brain, such as neuromodulation[33,34], β-amyloid plaque monitoring[31], and immune cell responses[32], can also be investigated using this technique.

Protocol

All the following experimental procedures were approved by and conducted in accordance with the Norwegian Food and Safety Authority, Sunnybrook Research Institute's Animal Care Committee, and the Canadian Council on Animal Care.

1. Material preparation

1. Prepare the materials needed for the cranial window surgery and ultrasound-microbubble treatments. For chronic cranial windows, sterilized tools and materials, a sterile surgical space, and pre- and post-surgery drug administration are necessary[23,24,25].
2. Transducer and coverslip preparation
    1. Check the physical integrity of the transducer: look for cracks and dents. Ensure the electrodes on the top and side of the transducer are intact.
    2. Deposit cyanoacrylate glue into a small dish. Use an applicator to spread a thin layer of glue onto the surface of the transducer.
    3. Place the transducer onto the glass coverslip. Press down firmly for 20-30 s.
        NOTE: A 3D-printed mold can be used to facilitate the alignment of the glass coverslip with the ring transducer, ensuring firm and even pressure on the coverslip and ring transducer (**Figure 2**).
    4. Check for bubbles between the transducer and the coverslip. If there are bubbles, take the coverslip off and repeat from step 1.2.3., as air impedes ultrasound propagation. Cure overnight at room temperature.
    5. Once adhered to a glass coverslip, match the transducer (**Figure 3**).
        NOTE: This protocol uses an in-house manufactured lead zirconate titanate ring transducer (10 mm outer diameter, 1.4 mm thickness, 1.2 mm height)[35], matched to a 50 Ω impedance and 0° phase load with a custom matching circuit. The transducer is driven at 0.82 MHz in thickness mode, producing a circular focal spot approximately 1 mm beneath the coverslip. Ring transducers of similar properties (10 mm outer diameter, 1.5 mm thickness, 1.1 mm height) have been characterized[26] and used extensively for multiphoton microscopy experiments[27,28,29,31,32,36].
3. Transducer reuse and coverslip replacement

1. Replace the coverslip if it is cracked or has debris (e.g., fur, glue) from the previous experiment. To remove the coverslip, dissolve the glue by submerging the transducer and coverslip in acetone for 20 min.

   NOTE: Acetone may affect the integrity of the transducer and/or electrodes. Check with the manufacturer before proceeding with this step.

2. Check if the acetone has dissolved the glue by gently pulling on the coverslip with forceps. Check once every 10 min to avoid prolonged acetone exposure.

2. Animal preparation

1. Anesthetize the animal by using a mix of medical air, oxygen, and isoflurane in an induction chamber.

   NOTE: Use of oxygen as a carrier gas has been reported to affect the half-life of microbubbles[37,38] and diminish the magnitude of ultrasound-microbubble induced increases in BBB permeability[27], but may also reduce the risk of hypoxia and mortality[39]. Choose carrier gases based on project aims and veterinarian advice. Injectable anesthetics such as a ketamine/xylazine cocktail may also be used; however, it is easier to control the plane of anesthesia and blood oxygen levels when using inhalable anesthetics.

2. Check that the animal has achieved a sufficient plane of anesthesia by performing a toe pinch. Weigh the animal to determine the dosage of dextran, microbubbles, and drugs to administer. Remove the fur from animal's head and place the animal onto a stereotactic frame.

3. For acute experiments, access to the systemic circulation must be established for dextran and microbubble injections. To achieve this, insert a 27 g catheter into a tail vein.

   NOTE: While retro-orbital injections are also possible, tail veins are recommended due to the limited working space in the head area during multiphoton imaging.

4. Transfer the animal onto the stereotactic frame and switch the anesthesia to the nose cone. Maintain the animal's core temperature of 37 °C using a heat source, such as a heating pad or a glove filled with warm water.

5. Monitor animal temperature by using a rectal probe, and animal physiology by using a pulse oximeter. Apply ophthalmic ointment. Inject appropriate pre-surgery analgesic and/or anti-inflammatory drugs (see **Table of Materials**).

6. Prior to starting the cranial window surgery, check the plane of anesthesia and the animal's heart rate, O_2 saturation, respiratory rate, and temperature.

7. To begin the cranial window surgery, remove the fur on the head by applying a depilatory cream and/or using fur clippers. Remove the fur from between the eyes to the anterior half of the neck (**Figure 4A**).

   NOTE: Prolonged contact with the depilatory cream will burn the skin. For chronic cranial window surgeries, wash the scalp with alternating wipes of betadine and 70% EtOH following fur removal. Prepare the surgical space for sterile surgery. Sterility must be maintained until Step 2.15.

8. To remove the scalp, lift the skin between the eyes using forceps held in the non-dominant hand, along the sagittal suture. Using curved scissors, remove the skin to expose the parietal bones (**Figure 4B**). Apply firm pressure with a cotton swab if there is bleeding from the skull or scalp;

bleeding must be stopped before progressing to the next step.

NOTE: For acute surgeries, the skin can be pushed back and adhered to the skull using liquid cyanoacrylate glue or tissue adhesive.

9. Remove the periosteum covering the outer surface of the skull using cotton swabs.

10. Using an operating microscope (6-25x) and a dental drill (0.5 mm drill burr, medium speed), outline a circle onto the parietal bone to mark the desired location of the cranial window on the skull (**Figure 5**). Avoid the sagittal suture, lambda, and bregma, as these areas are thinner and overlay large blood vessels.

    NOTE: To facilitate drilling, an outline of the cranial window can be drawn onto the skull using a marker and stencil (**Figure 5A**). For rats, it may be easier to drill a rectangular, instead of a circular, cranial window. Due to the thickness of the rat skull bone, use a 0.7 mm drill bit to outline the cranial window in the compact bone prior to using a 0.5 mm drill bit to complete the drilling process.

11. Apply gentle pressure with the drill bit; excessive pressure increases the risk of causing damage to brain tissue. To prevent the skull from overheating during drilling, drip saline onto the skull using a syringe, or apply a piece of surgical sponge soaked in saline.

12. Alternate between drilling and cooling the skull until the resulting bone island separates from the rest of the skull. Check the drilling progress by applying gentle pressure onto the bone island using forceps or the drill bit. Continue drilling until the bone island separates from the rest of the skull.

    NOTE: Small cracks in the thinnest areas of the skull are a good indication that drilling is almost complete. Attempting to remove the bone island prematurely can cause pieces of bone to penetrate into the brain tissue, damaging the dura and causing inflammation and bleeding.

13. Remove the bone island by using a pair of fine forceps to grasp the edges, or the upper compact bone layer, of the bone island (**Figure 6A**). Ensure that the brain is kept moist by applying a piece of surgical sponge that has been pre-soaked in saline. If bleeding is observed, place the surgical sponge on the region that is bleeding. Do not proceed to the next step until bleeding has ceased.

    NOTE: If bleeding persists after 5 min, the animal cannot be used for multiphoton imaging experiments. For rats, it may be necessary to remove the dura if it is thick. To remove the dura, use high magnification on the operating microscope and a pair of fine forceps.

14. To place a cranial window, pick up a glass coverslip with a pair of forceps, place a drop of saline onto one side, and maneuver it over the hole in the skull. Ensure that there are no air bubbles under the coverslip.

    NOTE: Use a 5 mm glass coverslip for mice, and 8 mm for rats. For rats, due to the thickness of the skull bone, use an agarose solution instead of saline to fill in the space between the coverslip and brain. The transducer and its coverslip can also be adhered directly onto the skull, instead of using a separate coverslip for the cranial window. For this option, proceed to step 3.1. Refer to **Figure 1** for details.

15. Spread a layer of cyanoacrylate glue around the perimeter of the coverslip (**Figure 6B**) to attach it to the skull. Ensure that there is no glue under the coverslip. Apply pressure onto the coverslip to ensure that glue does not come into contact with the brain.

16. Once the glue is completely dry, even out the surface of the glue by using the dental drill. Ensure all glue debris is removed from the surgical area.
    NOTE: For chronic cranial windows, inject the necessary post-surgical drugs (see Table of Materials), provide ointment for wound care and soft foods, and recover the animal under a heat lamp.

3. Placement of the ring transducer

1. Prepare the 1% (w/v) agarose solution. In a small beaker or Erlenmeyer flask, add 0.1 g of agarose and 10 mL of PBS (1x) or saline. Boil the solution until the agarose has fully dissolved by placing the beaker onto a hotplate or heating the solution in a microwave oven (30-45 s).
2. Steps 3.2-3.5 are time-sensitive as the agarose solution cools quickly. Withdraw ~ 0.5 mL of agarose into a 1 mL syringe.
    NOTE: To protect the integrity of the brain, ensure that the temperature of the agarose approximates body temperature before use.
3. Deposit the agarose liberally onto the coverslip of the cranial window.
    NOTE: If the tissue blanches, the temperature of the agarose was too high; the animal must be euthanized. If there is no separate coverslip covering the brain (i.e., the transducer and its coverslip are placed directly onto the brain, see step 2.14), then agarose should be deposited onto the surface of the brain in this step.
4. Place the transducer over the cranial window (**Figure 6C**). Apply firm pressure such that there is minimal agarose between the transducer and the cranial window. Ensure that the transducer is centered (XY-plane) and parallel (Z-plane) to the cranial window, and that there are no air bubbles in the agarose.
5. When the agarose has cooled to a jello-like consistency, cut away excess agarose from the circumference of the transducer's coverslip using a spatula or scalpel. Ensure that there are no air bubbles underneath the transducer's coverslip.
6. Using a spatula, spread a layer of cyanoacrylate glue over the circumference of the transducer's coverslip, extending to the skull, such that the transducer is firmly adhered to the skull.
7. Maintain firm pressure on the transducer until the glue has completely dried (10-15 min).

4. Multiphoton microscopy imaging

1. Position the animal under the objective lens (**Figure 7A**). Ensure that the objective lens is centered in the ring transducer, and parallel with the transducer (**Figure 7B**). If a water-immersion objective lens is used, fill the center of the ring transducer with deionized and degassed water.
    NOTE: Degassed water is important for proper ultrasound propagation.
2. Start with the objective lens in its highest position, and then slowly lower the objective lens until it is within the ring transducer (**Figure 7A, B**). Ensure that objective lens does not collide with the transducer or coverslip.
    NOTE: Alternate between the eyepiece to check if the Z-position of the objective lens is in-plane with the surface of the brain, and by eye to ensure that the objective lens does not collide with the transducer or coverslip. It may be easier to visualize the pial vessels through

the eyepiece following injection of fluorescent dextran through the tail vein (**Figure 7C**).

3. Prepare the multiphoton microscope for imaging.

   NOTE: This protocol uses an upright multiphoton microscope and a 20-25x objective lens that has a working distance of 2 mm, which is sufficient to focus beyond the coverslip(s), into the brain parenchyma.

4. Prepare the dextran. Add the appropriate amount of PBS to the vial of dextran, as per the manufacturer's instructions. Vortex the dextran solution for 1-3 min to ensure that the dextran powder is fully dissolved. Inject the dextran solution into the tail vein.

5. Setting up an image scan

   1. Using the eyepieces, ensure that the objective lens is parallel to the brain. Tilt the animal to correct for XZ and YZ misalignments.

   2. Select a field-of-view in a multiphoton microscope. Set up an XYZ scan before ultrasound exposure to have a baseline image of the vasculature prior to ultrasound exposure.

      NOTE: Typical imaging parameters are as follows: 300-800 µm in depth, 2-5 µm step-size, and 10-20 time stacks. Ensure that the objective lens does not come into contact with the transducer or coverslip at its lowest point during the imaging sequence.

5. Ultrasound exposure

1. Ensure all the BNC cables are connected correctly (**Figure 3**).

2. Set up an XYZT image scan that is sufficiently long enough to capture image stacks before, during, and after ultrasound-microbubble treatments.

3. Prepare the microbubbles by following the manufacturer's instructions. Inject the microbubbles into the tail vein and begin imaging.

   NOTE: Microbubble injections can be done with an infusion pump to ensure consistent injection rate and to enable concurrent microbubble injection and imaging. If microbubbles are to be injected during imaging, ensure that the tail vein can be easily accessed without exposing the detectors to ambient light.

4. Begin sonication.

   NOTE: Typical sonication parameters are as follows: 10 ms cycles, mechanical index of 0.2-0.4, and pulse repetition frequencies between 1-4 Hz. Sonication and microbubble parameters used in preclinical ultrasound-microbubble studies have been extensively studied and are well documented in literature (e.g. see [40] for a review).

5. Continue multiphoton imaging throughout the duration of sonication and following the end of sonication. Be observant for dextran extravasation from blood vessels, as this is indicative of increases in BBB permeability.

   NOTE: If dextran is detected in the extravascular space, but in the periphery of the field-of-view, then there may be affected blood vessels outside of the field-of-view. This can result from misalignment of the transducer with the focus of the objective lens. In this scenario, it is easier to adjust the field-of-view by moving the objective lens or by repositioning the animal, than to realign the transducer.

6. Once imaging is completed, euthanize the animal cervical dislocation under deep anesthesia or CO_2 asphyxiation. For chronic cranial windows, spread a layer of dental cement onto the exposed skull.

NOTE: For chronic cranial windows, the skin surrounding the window can be sutured, although this is not necessary, due to the removal of the scalp in step 2.8.

6. Image analysis

1. Export image stacks.
2. Analyze images with image analysis software (e.g., Olympus Fluoview, ImageJ/FIJI, Bitplane Imaris, ThermoFisher Scientific Amira) and/or programming tools (e.g., Python, MATLAB).

Representative Results

Successful ultrasound-microbubble treatments can be detected by the extravasation of fluorescent dextran from the intravascular to the extravascular space (**Figure 8**), indicating an increase in BBB permeability. Depending on the pressure field of the ring transducer, pial vessels and/or capillaries will be affected.

To evaluate the vascular changes induced by ultrasound-microbubble treatments, the diameter of the vessel of interest can be measured before, during, and after ultrasound-microbubble treatment (**Figure 9**). This can be done manually in a commercially available software (e.g., Olympus Fluoview software). During image acquisition, bolus dextran injections and line scans can also be used to assess blood flow[30,41]. To evaluate kinetics of dextran leakage as a representative model for drug delivery, the signal intensity between the intra- and extravascular spaces can be evaluated using tools such as MATLAB[26,27,29,41] (**Figure 10**).

Further image processing can be achieved using ImageJ/FIJI. ImageJ/FIJI is an open-source software that is compatible with MATLAB and is well-suited to conduct common analyses in biological image analysis, such as measuring vascular changes, or the lengths of or distance between fluorescent objects (e.g., β-amyloid plaques to blood vessels). Image processing pipelines created in ImageJ/FIJI can be automated by writing custom macros.

More complex analyses, such as 3D segmentation of blood vessels and cell tracking, can be achieved using more advanced, semi-automated software (**Figure 11**). Following segmentation, more specific analyses can be conducted, such as classifying blood vessels as arterioles, venules, or capillaries, based on diameter, branching, tortuosity patterns, and flow direction[42,43]. Machine learning algorithms have also been developed to automate blood vessel segmentation[22,44].

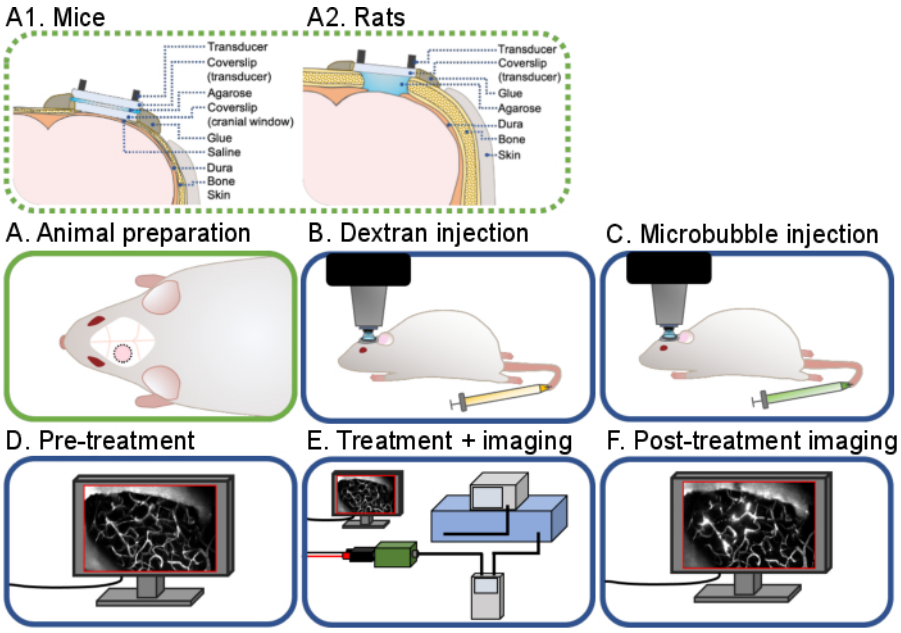

Figure 1: General workflow of intravital multiphoton ultrasound-microbubble brain experiments. A general workflow of the intravital multiphoton ultrasound-microbubble brain experiments described in this protocol is shown. There are 6 steps: (**A**) Animal preparation for (**A1**) mice and (**A2**) rats, (**B**) Dextran injection, (**C**) Microbubble injection, (**D**) Pre-treatment imaging, (**E**) Treatment and imaging, (**F**) Post-treatment imaging and data analysis. Please click here to view a larger version of this figure.

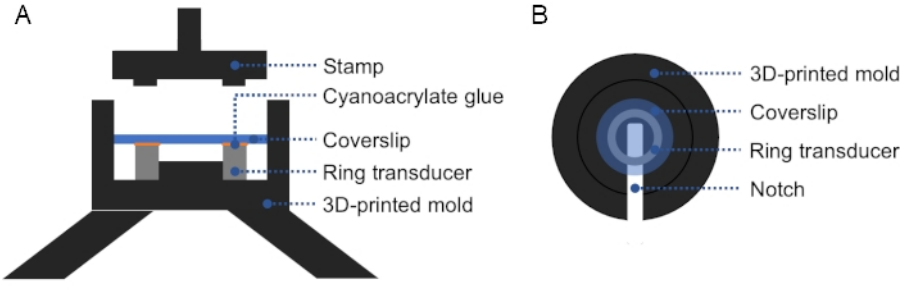

Figure 2: Cross-section and top view of 3D-printed mold. (**A**) Cross-section of the mold. A thin layer of cyanoacrylate glue is applied on the top surface of the ring transducer, and a coverslip is placed on top. A stamp may be used to apply firm, even pressure on the coverslip and ring transducer. (**B**) Top view of the mold. A notch can be added in the mold to facilitate removal of the prepared transducer. Please click here to view a larger version of this figure.

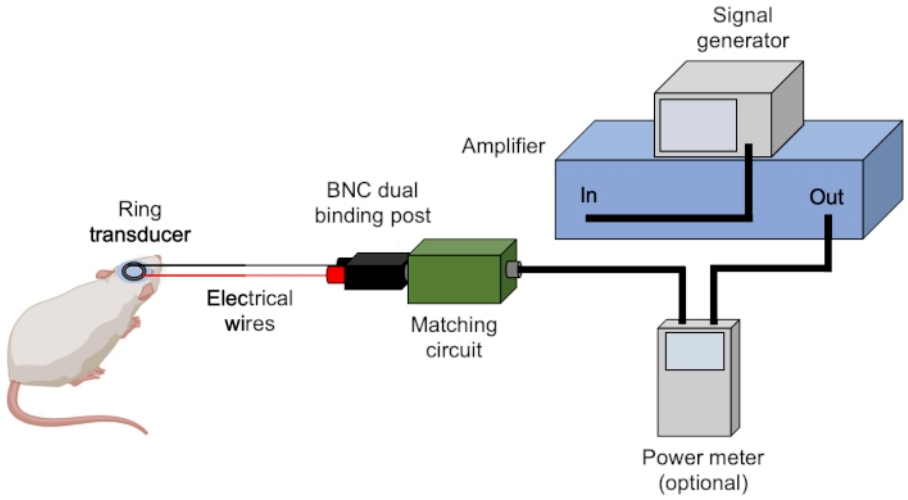

Figure 3: Ultrasound set-up. Typical hardware for ultrasound experiments are shown. Ultrasound parameters are set and triggered by the signal generator and amplified by the amplifier. A power meter can be used to record forward and reflected powers prior to sending the signal to the matching box, which is matched to the transducer. All connections are achieved using BNC cables unless stated otherwise. Please click here to view a larger version of this figure.

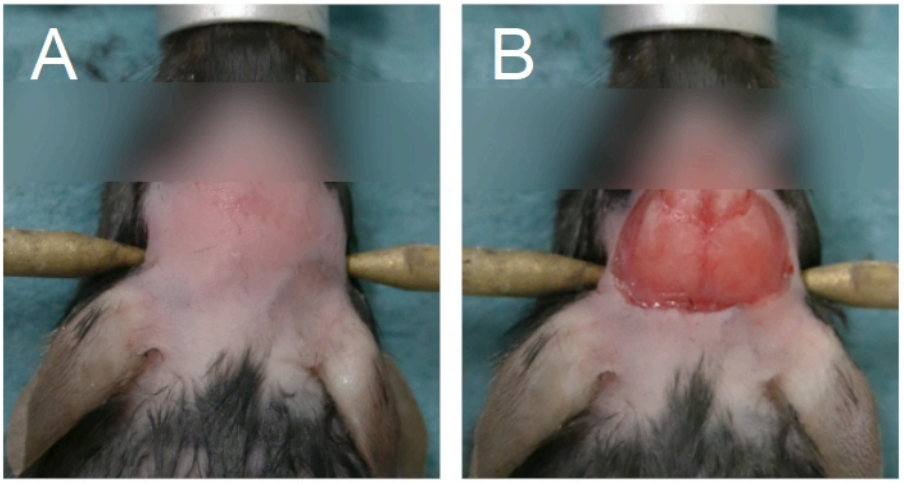

Figure 4: Area of fur removal and scalp removal. (**A**) Fur removal should start from between the eyes and extend until the anterior half of the neck. (**B**) Scalp removal should be sufficient to expose the parietal bones. Bleeding must be stopped before proceeding. Please click here to view a larger version of this figure.

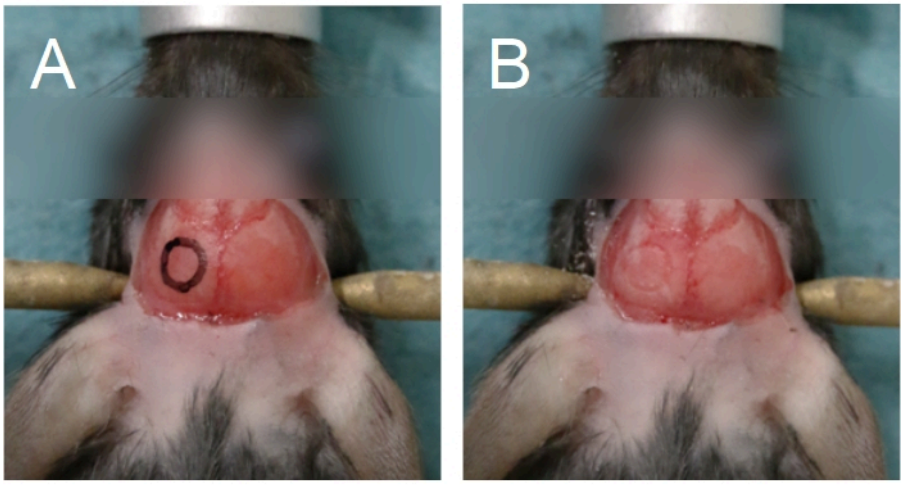

Figure 5: Outline of the cranial window. The cranial window is situated on a parietal bone. (**A**) An outline of the cranial window can be drawn onto the skull to aid in the drilling process. (**B**) The outline of the cranial window can be seen following drilling through the compact bone. Please click here to view a larger version of this figure.

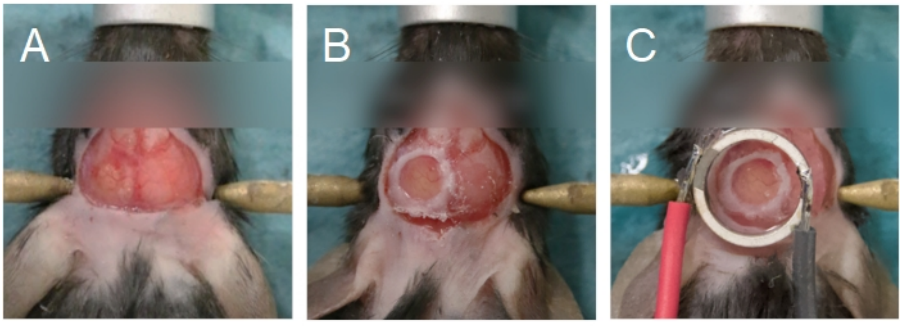

Figure 6: Cranial window and transducer alignment. (**A**) The cranial window is created on a parietal bone. The bone island has been removed, exposing the brain underneath. (**B**) The cranial window is complete when a glass coverslip is sealed onto the skull using cyanoacrylate glue. (**C**) The transducer is centered to the cranial window and adhered using cyanoacrylate glue. Please click here to view a larger version of this figure.

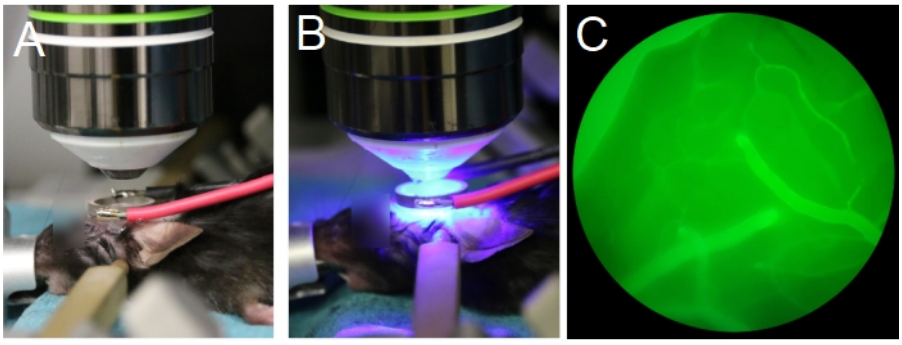

Figure 7: Positioning of objective lens and transducer. (**A**,**B**) The objective lens is centered to the ring transducer. (**C**) Blood vessels filled with fluorescent dextran are visible through the eyepieces, under epifluorescence. Please click here to view a larger version of this figure.

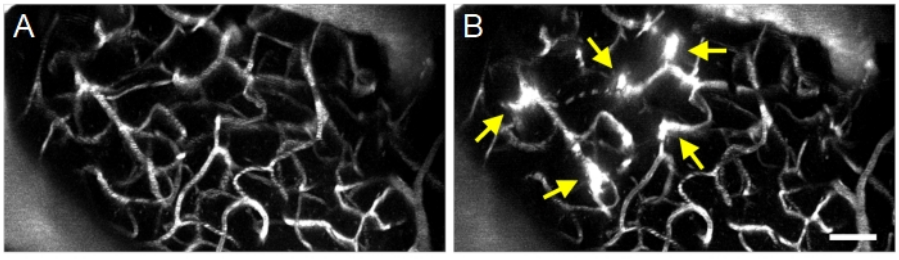

Figure 8: Maximum projection multiphoton images of ultrasound-microbubble induced increases in BBB permeability. Maximum projection images of vasculature (**A**) before and (**B**) after ultrasound-microbubble treatments. Successful ultrasound-microbubble treatments can be confirmed by observing increases in BBB permeability following treatment, visualized as fluorescent dextran extravasation (arrows). Scale bar: 50 µm. Please click here to view a larger version of this figure.

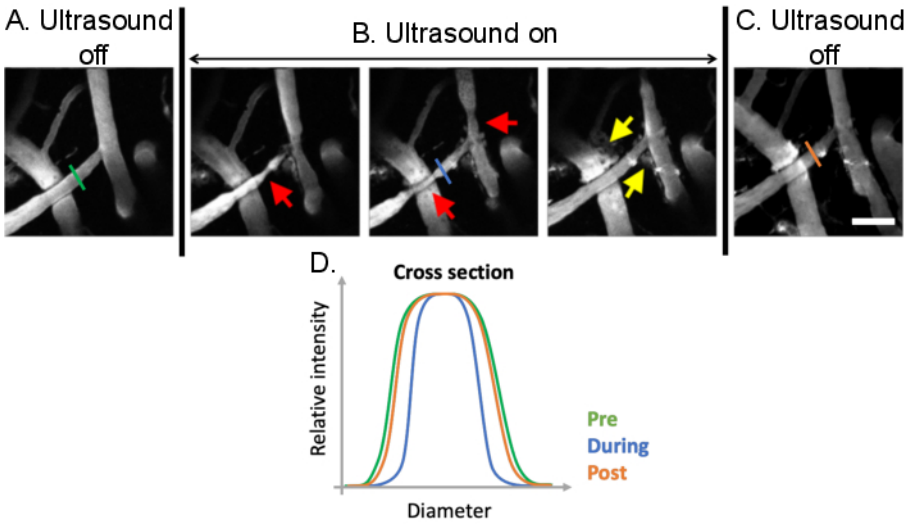

Figure 9: Analysis of vasomodulation induced by ultrasound-microbubble treatments. Maximum projection images of cerebral blood vessels before, during, and after ultrasound-microbubble treatments. Microbubbles are present in all images. Compared to (**A**) pre-treatment conditions, clear vasomodulation can be observed (**B**) during ultrasound-microbubble treatments (red arrows). Ultrasound-microbubble mediated increases in BBB permeability are also evident following treatment from the leakage of fluorescent dextran from the intravascular to the extravascular space (yellow arrows). (**C**) When ultrasound is turned off, vascular diameters return to pre-treatment, baseline sizes. (**D**) Vascular changes can be analyzed by plotting the diameter of the vessel of interest before, during, and after ultrasound-microbubble treatment. Scale bar: 100 µm. (Unpublished work). Please click here to view a larger version of this figure.

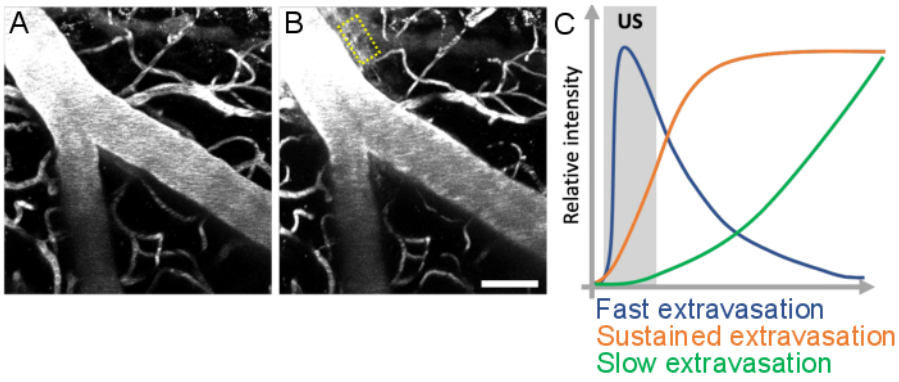

Figure 10: Analysis of leakage kinetics following ultrasound-microbubble treatments. Increase in BBB permeability is visualized as leakage of fluorescent dextran from the intravascular to the extravascular space. Changes in BBB permeability are evident when comparing image stacks acquired (**A**) before and (**B**) after ultrasound-microbubble treatments. (**C**) Leakage kinetics can be analyzed by tracking the intensity, volume, and speed of dextran in extravascular compartments (yellow rectangle). Scale bar: 50 µm. (Unpublished work.) Please click here to view a larger version of this figure.

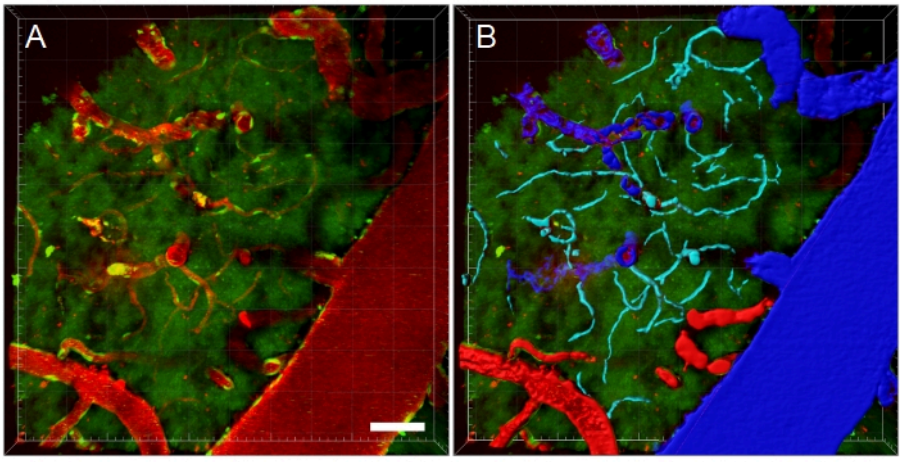

Figure 11: Blood vessel segmentation of multiphoton microscopy XYZ stack. (**A**) Depth (XYZ) stack of blood vessels in a transgenic EGFP rat. Blood vessels are visualized via intravenous injection of fluorescent Texas Red 70 kDa dextran (red). The green channel shows fluorescent cells and tissue autofluorescence. (**B**) 3D reconstructions of blood vessels are created, and then color-coded according to blood vessel type to facilitate type-specific analyses. Vein/venules are blue, arteries/arterioles are red, and capillaries are cyan. Scale bar: 50 µm. Reconstructions created using Bitplane Imaris. Please click here to view a larger version of this figure.

Discussion

Intravital multiphoton microscopy monitoring of the brain is a valuable tool to study brain responses during ultrasound exposure. To our knowledge, the protocol described here is the only method of conducting multiphoton microscopy imaging of the brain parenchyma during ultrasound-microbubble treatments. The creation of cranial windows and the use of ring transducers allow real-time monitoring of vascular, cellular, and other downstream responses to ultrasound-microbubble treatments at high spatial and temporal resolution. Other groups have performed multiphoton microscopy imaging following the completion of ultrasound-microbubble treatments, thereby missing the real-time response of the brain parenchyma to treatments[19]. The procedure described offers improved temporal control, allowing the collection of data that may help illuminate the acute mechanisms behind ultrasound-microbubble treatments. Quantitative and qualitative data can be extracted and analyzed from the acquired image stacks, such as extravasation kinetics[27,29,30], changes in β-amyloid plaque volume[31], and cell dynamics[32].

Several troubleshooting steps were highlighted throughout the protocol. First, surgical steps that are particularly susceptible to operator error were emphasized, such as use of agarose during cranial window surgery and placement of the transducer. Steps to prevent animal discomfort and death were also provided, including monitoring animal physiology during surgery, and thoroughly vortexing the dextran prior to injection. Second, physical specifications of the transducer, and alignment of the objective lens, transducer, and cranial window, were also highlighted. The specifications of the ring transducer and its acoustic properties must be determined in consideration of the objective lens used as well as the animal model. Specifically, the inner diameter of the ring transducer must be large enough to surround the objective lens, but small enough to be mounted securely onto the animal's skull. In addition, the focal area of the transducer must align with the range of the objective lens used.

A common challenge is that the cranial window and ring transducer are angled relative to the objective lens. Proper centering (XY) and alignment (Z) of the objective lens with the cranial window and transducer ensures that the focal area of the transducer, and thus the region of treated brain tissue, aligns with the imaging field-of-view, and reduces the risk of collision between the objective lens and transducer during imaging. Alignment can be achieved by adjusting the head position of the animal and/or by rotating the stereotactic frame that it is fixed in.

Microscope components (e.g., detectors, beam splitters) and image acquisition parameters should be selected based on the aim of the study. Here, an objective lens with a long focal length (> 2 mm) is used due to the presence of the coverslip(s) and ring transducer located between the objective lens and the brain. An upright microscope is also recommended as it allows for more space to maneuver the animal, particularly for brain experiments. To capture the kinetics of ultrasound-microbubble induced leakage of the intravascular dye, a high temporal resolution is favorable, which can be achieved by using a resonance scanning system. Combining this with a high sensitivity detection system, such as gallium arsenide phosphide (GaAsP) detectors, will also result in more favorable images.

The experimental procedure presented has several limitations. First, the surgical procedure is quite invasive, and has been reported to cause inflammation[45], although inflammation can be minimized[46]. Moreover, immune responses induced by cranial window surgeries were

observed to resolve by 2-4 weeks following surgery[23,24,25]. In addition, the drilling process, particularly when conducted with excessive force or speed, can cause damage to underlying tissue due to the generation of heat, vibration, and pressure applied. Cranial window surgeries and multiphoton imaging have also been observed to affect brain temperature[47]. These limitations can be reduced to an extent through careful creation of pristine cranial windows, proper recovery of animals with chronic cranial windows, and maintenance of normothermic body temperature using a heating source with feedback control. Second, the imaging depth is limited by the microscope and objective lens used. For example, the effect of ultrasound-microbubble treatment in deeper brain structures, such as the hippocampus, cannot be studied without more invasive measures, such as the removal of overlying cortical tissue[48], or the use of microlenses in conjunction with cortical penetration[49]. Using an objective lens with a long working distance could resolve this issue to an extent, but light penetration is also limited at greater depths.

While the representative images of this protocol were acquired from wild-type rodents, the presented experimental procedure can also be applied to transgenic animals and disease models, such as Alzheimer's disease[31]. Ultrasound experiments unrelated to BBB modulation, such as ultrasound-induced neuromodulation, can also be monitored using this protocol[33,34]. Other possible applications can be achieved by using different microscope or detector set-ups, such as pairing a confocal microscope with an ultra-high-speed camera[50]. While photobleaching and phototoxicity are comparatively worse in confocal microscopes due to the large excitation volume, ultra-high-speed imaging may enable visualization of brain capillary endothelial cell-microbubble interactions with high temporal resolution, which could further illuminate the mechanisms driving ultrasound-microbubble BBB treatments. To conclude, the protocol described provides a method to monitor vascular and cellular effects induced by ultrasound-microbubble BBB experiments in real-time, providing a tool to further determine the mechanisms driving these treatments, as well as illuminating the downstream responses of the brain parenchyma to ultrasound-microbubble treatments.

Disclosures

Charissa Poon, Melina Mühlenpfordt, Marieke Olsman, and Catharina de Lange Davies declare no financial nor non-financial competing conflicts of interest. Spiros Kotopoulis is a full-time employee and owns shares in EXACT Therapeutics AS, a company developing ultrasound and microbubble/cluster enhanced drug delivery. Kullervo Hynynen is the founder of FUS Instruments, from which he receives non-research related support.

Acknowledgments

Housing of the animals was provided by the Comparative Medicine Core Facility (CoMed, NTNU). Figure 3 was created in BioRender.com. Video recording and editing was done by Per Henning, webmaster at the Faculty for Natural Science at NTNU. The project was funded by the Norwegian University of Science and Technology (NTNU, Trondheim, Norway), Research Council of Norway (RCN 262228), Canadian Institutes of Health Research (FDN 154272), National Institute of Health (R01 EB003268), and the Temerty Chair in Focused Ultrasound Research at Sunnybrook Health Sciences Centre.

References

1. Abbott, N. J., Rönnbäck, L., Hansson, E. Astrocyte-endothelial interactions at the blood-brain barrier. *Nature Reviews Neuroscience.* **7** (1), 41-53 (2006).
2. Kalladka, D. et al. Human neural stem cells in patients with chronic ischaemic stroke (PISCES): a phase 1, first-in-man study. *Lancet (London, England).* **388** (10046), 787-796 (2016).
3. Pardridge, W. M. The blood-brain barrier: Bottleneck in brain drug development. *NeuroRx : the journal of the American Society for Experimental NeuroTherapeutics.* **2** (1), 12 (2005).
4. Lochhead, J. J., Thorne, R. G. Intranasal delivery of biologics to the central nervous system. *Advanced Drug Delivery Reviews.* **64** (7), 614-628 (2012).
5. Nagy, Z., Pappius, H. M., Mathieson, G., Hüttner, I. Opening of tight junctions in cerebral endothelium. I. Effect of hyperosmolar mannitol infused through the internal carotid artery. *The Journal of Comparative Neurology.* **185** (3), 569-578 (1979).
6. Hynynen, K., McDannold, N., Vykhodtseva, N., Jolesz, F. A. Noninvasive MR imaging-guided focal opening of the blood-brain barrier in rabbits. *Radiology.* **220** (3), 640-646 (2001).
7. Burgess, A. et al. Alzheimer disease in a mouse model: MR imaging-guided focused ultrasound targeted to the hippocampus opens the blood-brain barrier and improves pathologic abnormalities and behavior. *Radiology.* **273** (3), 736-745 (2014).
8. Abrahao, A. et al. First-in-human trial of blood-brain barrier opening in amyotrophic lateral sclerosis using MR-guided focused ultrasound. *Nature Communications.* **10** (1), 4373 (2019).
9. Hynynen, K., Jones, R. M. Image-guided ultrasound phased arrays are a disruptive technology for non-invasive therapy. *Physics in Medicine and Biology.* **61** (17), R206-248 (2016).
10. Burgess, A. et al. Targeted delivery of neural stem cells to the brain using MRI-guided focused ultrasound to disrupt the blood-brain barrier. *PLoS One.* **6** (11), e27877 (2011).
11. McDannold, N., Arvanitis, C. D., Vykhodtseva, N., Livingstone, M. S. Temporary disruption of the blood-brain barrier by use of ultrasound and microbubbles: Safety and efficacy evaluation in rhesus macaques. *Cancer Research.* **72** (14), 3652-3663 (2012).
12. Downs, M.E. et al. Long-term safety of repeated blood-brain barrier opening via focused ultrasound with microbubbles in non-human primates performing a cognitive task. *PLOS One.* **10** (5), e0125911 (2015).
13. Baghirov, H. et al. Ultrasound-mediated delivery and distribution of polymeric nanoparticles in the normal brain parenchyma of a metastatic brain tumour model. *PloS One.* **13** (1), e0191102 (2018).
14. Sulheim, E. et al. Therapeutic effect of cabazitaxel and blood-brain barrier opening in a patient-derived glioblastoma model. *Nanotheranostics.* **3** (1), 103-112 (2019).
15. Bing, C. et al. Transcranial opening of the blood-brain barrier in targeted regions using a stereotaxic brain atlas and focused ultrasound energy. *Journal of Therapeutic Ultrasound.* **2**, 13 (2014).
16. O'Reilly, M.A., Hynynen, K. Blood-brain barrier: Real-time feedback-controlled focused ultrasound disruption

by using an acoustic emissions-based controller. *Radiology.* **263** (1), 96-106 (2012).

17. Jones, R. M., Deng, L., Leung, K., McMahon, D., O'Reilly, M.A., Hynynen, K. Three-dimensional transcranial microbubble imaging for guiding volumetric ultrasound-mediated blood-brain barrier opening. *Theranostics.* **8** (11), 2909-2926 (2018).
18. Jones, R. M., McMahon, D., Hynynen, K. Ultrafast three-dimensional microbubble imaging *in vivo* predicts tissue damage volume distributions during nonthermal brain ablation. *Theranostics.* **10** (16), 7211-7230 (2020).
19. Arvanitis, C. D. et al. Mechanisms of enhanced drug delivery in brain metastases with focused ultrasound-induced blood-tumor barrier disruption. *Proceedings of the National Academy of Sciences.* **115** (37), E8717-E8726 (2018).
20. Shih, A.Y. et al. Two-photon microscopy as a tool to study blood flow and neurovascular coupling in the rodent brain. *Journal of Cerebral Blood Flow and Metabolism.* 33 (2012).
21. McCarter, J. F. et al. Clustering of plaques contributes to plaque growth in a mouse model of Alzheimer's disease. *Acta Neuropathologica.* **126** (2), 179-188 (2013).
22. Cruz Hernández, J. C. et al. Neutrophil adhesion in brain capillaries reduces cortical blood flow and impairs memory function in Alzheimer's disease mouse models. *Nature Neuroscience.* **22** (3), 413-420 (2019).
23. Holtmaat, A. et al. Long-term, high-resolution imaging in the mouse neocortex through a chronic cranial window. *Nature Protocols.* **4** (8), 1128-1144 (2009).
24. Goldey, G. J. et al. Removable cranial windows for long-term imaging in awake mice. *Nature Protocols.* **9** (11), 2515-2538 (2014).
25. Cao, V. Y. et al. *In vivo* two-photon imaging of experience-dependent molecular changes in cortical neurons. *Journal of Visualized Experiments.* (71), 50148 (2013).
26. Nhan, T., Burgess, A., Hynynen, K. Transducer design and characterization for dorsal-based ultrasound exposure and two-photon imaging of *in vivo* blood-brain barrier disruption in a rat model. *IEEE Transactions on Ultrasonics, Ferroelectrics, and Frequency Control.* **60** (7), 1376-1385 (2013).
27. Cho, E. E., Drazic, J., Ganguly, M., Stefanovic, B., Hynynen, K. Two-photon fluorescence microscopy study of cerebrovascular dynamics in ultrasound-induced blood-brain barrier opening. *Journal of Cerebral Blood Flow & Metabolism.* **31** (9), 1852-1862 (2011).
28. Burgess, A., Nhan, T., Moffatt, C., Klibanov, A. L., Hynynen, K. Analysis of focused ultrasound-induced blood-brain barrier permeability in a mouse model of Alzheimer's disease using two-photon microscopy. *Journal of Controlled Release.* **192**, 243-248 (2014).
29. Nhan, T. et al. Drug delivery to the brain by focused ultrasound induced blood-brain barrier disruption: Quantitative evaluation of enhanced permeability of cerebral vasculature using two-photon microscopy. *Journal of Controlled Release.* **172** (1), 274-280 (2013).
30. Nhan, T., Burgess, A., Lilge, L., Hynynen, K. Modeling localized delivery of Doxorubicin to the brain following focused ultrasound enhanced blood-brain barrier permeability. *Physics in Medicine and Biology.* **59** (20), 5987-6004 (2014).

31. Poon, C. T. et al. Time course of focused ultrasound effects on β-amyloid plaque pathology in the TgCRND8 mouse model of Alzheimer's disease. *Scientific Reports.* **8** (1), 14061 (2018).
32. Poon, C., Pellow, C., Hynynen, K. Neutrophil recruitment and leukocyte response following focused ultrasound and microbubble mediated blood-brain barrier treatments. *Theranostics.* **11** (4), 1655-1671 (2021).
33. Tufail, Y. et al. Transcranial pulsed ultrasound stimulates intact brain circuits. *Neuron.* **66** (5), 681-694 (2010).
34. Chu, P.-C. et al. Neuromodulation accompanying focused ultrasound-induced blood-brain barrier opening. *Scientific Reports.* **5** (1), 15477 (2015).
35. Yddal, T., Kotopoulis, S., Gilja, O. H., Cochran, S., Postema, M. *Transparent glass-windowed ultrasound transducers.* 2079-2082, at <http://eprints.gla.ac.uk/158176/> (2014).
36. Santos, M. A., Goertz, D. E., Hynynen, K. Focused ultrasound hyperthermia mediated drug delivery using thermosensitive liposomes and visualized with *in vivo* two-photon microscopy. *Theranostics.* **7** (10), 2718-2731 (2017).
37. Mullin, L. et al. Effect of anesthesia carrier gas on *in vivo* circulation times of ultrasound microbubble contrast agents in rats. *Contrast Media & Molecular Imaging.* **6** (3), 126-131 (2011).
38. Itani, M., Mattrey, R. F. The effect of inhaled gases on ultrasound contrast agent longevity *in vivo. Molecular Imaging and Biology.* **14** (1), 40-46 (2012).
39. Baum, J. A. The carrier gas in anaesthesia: Nitrous oxide/oxygen, medical air/oxygen and pure oxygen. *Current Opinion in Anaesthesiology.* **17** (6), 513-516 (2004).
40. Poon, C., McMahon, D., Hynynen, K. Noninvasive and targeted delivery of therapeutics to the brain using focused ultrasound. *Neuropharmacology.* **120**, 20-37 (2017).
41. Joo, I. L. et al. Early neurovascular dysfunction in a transgenic rat model of Alzheimer's disease. *Scientific Reports.* **7**, 46427 (2017).
42. Dorr, A. et al. Amyloid-β-dependent compromise of microvascular structure and function in a model of Alzheimer's disease. *Brain: A Journal of Neurology.* **135** (Pt 10), 3039-3050 (2012).
43. Kim, T. N. et al. Line-scanning particle image velocimetry: An optical approach for quantifying a wide range of blood flow speeds in live animals. *PLOS One.* **7** (6), e38590 (2012).
44. Teikari, P., Santos, M., Poon, C., Hynynen, K. Deep learning convolutional networks for multiphoton microscopy vasculature segmentation. *arXiv:1606.02382 [cs].* at <http://arxiv.org/abs/1606.02382> (2016).
45. Denes, A. et al. Surgical manipulation compromises leukocyte mobilization responses and inflammation after experimental cerebral ischemia in mice. *Frontiers in Neuroscience.* **7**, e00271 (2014).
46. Koletar, M. M., Dorr, A., Brown, M. E., McLaurin, J., Stefanovic, B. Refinement of a chronic cranial window implant in the rat for longitudinal *in vivo* two-photon fluorescence microscopy of neurovascular function. *Scientific Reports.* **9** (1), 5499 (2019).
47. Podgorski, K., Ranganathan, G. Brain heating induced by near-infrared lasers during multiphoton microscopy. *Journal of Neurophysiology.* **116** (3), 1012-1023 (2016).

48. Ulivi, A. F. et al. Longitudinal two-photon imaging of dorsal hippocampal CA1 in live mice. *Journal of Visualized Experiments: JoVE.* (148), e59598 (2019).

49. Levene, M. J., Dombeck, D. A., Kasischke, K. A., Molloy, R. P., Webb, W. W. *In vivo* multiphoton microscopy of deep brain tissue. *Journal of Neurophysiology.* **91** (4), 1908-1912 (2004).

50. Beekers, I. et al. Combined confocal microscope and Brandaris 128 ultra-high-speed camera. *Ultrasound in Medicine & Biology.* **45** (9), 2575-2582 (2019).